Some design criteria in scanning tunneling microscopy

by Dieter W. Pohl

Optimum functioning of a scanning tunneling microscope (STM) requires tip-to-sample position control with picometer precision, a rough and fine positioning capability in three dimensions, a scanning range of at least 100 times the lateral resolution, a scanning speed as high as possible, and also, preferably, simplicity of operation. These requirements have to be satisfied in the presence of building vibrations with up to micrometer-size amplitudes, temperature drift, and other perturbations. They result in design rules, presented and discussed here, for the optimization of damping, stiffness, electrical control circuitry, and the performance of the piezoelectric actuators usually employed in STMs.

1. Introduction

In a well-designed STM, tip-to-sample position control should be better than the resolution desired: This is the condition *sine qua non* in scanning tunneling microscopy. For high-performance STMs [1], for which the recognition of individual surface atoms is the key design objective, a resolution is sought of about 0.1 Å normal to the sample surface (z direction), and about 1 Å laterally (x, y directions). This results in tolerance requirements of

$$\delta z \simeq 1 \text{ pm}, \tag{1a}$$

$$\delta x, \delta y \simeq 10 \text{ pm}. \tag{1b}$$

Here, we have switched to SI units (1 Å = 100 pm), which may be more appropriate to the forthcoming engineering-oriented discussion. Such narrow tolerance requirements, to the author's knowledge, are the smallest ever formulated for a mechanical device. They confront the designer with a number of new and challenging problems, and must be satisfied in the presence of various partially ill-defined disturbances such as building vibrations, acoustic noise, and temperature drift, as well as hysteresis and creep of the piezoelectric translation elements usually employed. Moreover, they must be met in the presence of four other mechanical design requirements, viz.,

2. Precision z distance regulation in the 0.1–1-μm range.
3. x and y scanning capability in the same range.
4. Tip approach $\tilde{z}$ in the 1-mm to 100-nm range.
5. Scan window selection $\tilde{x}$, $\tilde{y}$ in the same range.

Requirements 2 and 3 result from the need for three-dimensional tip-translation capability required to record surface topography. Requirements 4 and 5 emerge from the need for a capability for convenient sample loading, for reducing tip-to-sample separation from macroscopic to tunneling distances, and for selecting an area of interest on

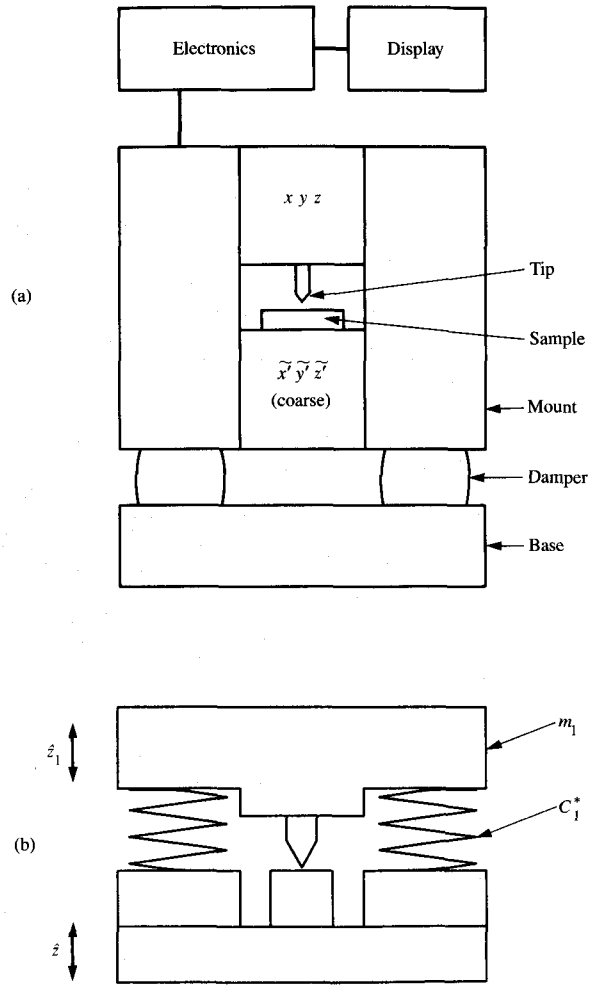

Figure 1

(a) Basic features of a typical STM, including two sets of three-dimensional translation stages and dampers. (b) Simple equivalent model.

the sample surface. To satisfy requirements 4 and 5 completely, a second set of three translational stages $\tilde{x}$, $\tilde{y}$, $\tilde{z}$ must be installed. Hence, a "complete" STM incorporates arrangements for six degrees of translational freedom with different ranges and precision as shown schematically in **Figure 1(a)**. [The equivalent model in Figure 1(b) is discussed later.] Since full $\tilde{x}$, $\tilde{y}$ spot-selection capability is not mandatory for all applications, most STMs built until now have been restricted to five degrees of freedom, omitting the somewhat complicated vertical translator for reasons of design simplicity.

The six (five) translations have to be performed with reasonable and coordinated speeds, not only to achieve efficient operation but also to minimize other disturbing influences such as thermal drift or surface modification by adsorption, etc. Finally, tolerance requirement 1 as well as requirements 2–5 must be satisfied with UHV-compatible design elements for high-end STMs. This greatly restricts the choice of materials and applicable techniques.

Perturbations causing uncontrolled variations in tip-sample position occur at considerably different time scales, and they couple differently to the mechanical parts of an STM. Suppression of their influence, therefore, requires a set of measures, in particular a high degree of stiffness and damping to deal with external vibrations (Section 2).

A major limitation to stiffness comes from the piezoelectric ceramic elements generally used for displacement. The manifold of translators introduces, as a result of their finite dimensions, a certain elastic "softness" to the STM which has to be balanced against the requirement of maximum stiffness for vibration insensitivity (Section 3).

Compensation for thermal expansion is needed in order to render an STM insensitive to temperature variations. Deviations from linearity of the piezoelectric ceramic elements can be minimized by appropriate choices of materials and translator designs. The electric fields required for their actuation should be kept as small as possible (Section 4).

Intimately related to the stiffness problem are optimum distance control by tunneling-current stabilization and maximum scanning speed (Section 5).

2. Stiffness, damping, and vibrations

• *Building vibrations*

Typically, buildings vibrate at frequencies between 10 and 100 Hz. These vibrations are excited by machines running at or near line frequency, and by the associated harmonics and subharmonics. The frame, walls, and floors of a building mostly undergo shear and bending (membrane) vibrations which usually resonate at frequencies between 15 and 25 Hz. These values are directly related to the maximum floor load, with standard values of 500–1000 kg/m^2 in modern buildings. The vibration spectra of buildings therefore frequently contain their largest maxima near the third subharmonic of the line frequency, i.e., 15 to 20 Hz, as in the example shown in **Figure 2**. The solid curve is an accelerometer record representing the vertical acceleration amplitude of a typical floor in our laboratory during the daytime. The acceleration values have to be divided by $(2\pi\nu)^2$—where ν is the frequency of vibration—to obtain the respective floor amplitudes (solid bars in Figure 2).

The largest peak appears near 17 Hz, with an amplitude of 0.2 μm. Amplitudes of up to 1 μm can be observed, depending on the distance from the beams of the concrete frame. The peaks at 50 and 100 Hz are much less pronounced, probably because they are off-resonance with

regard to the (lowest-order) floor eigenfrequency. The peak around zero is an instrumental artifact.

Attention must be paid not only to the continuous excitations shown in Figure 2, but also to the response of the floor to irregular motions such as those caused by persons walking and working in the laboratory. These excitations typically are in the 1–3-Hz range, with amplitudes comparable to the 17-Hz peak. They are indicated by the dashed bar in Figure 2.

In conclusion, in the process of minimization of the sensitivity of an STM to building vibrations, primary attention has to be given to the frequency range between 1 and 100 Hz.

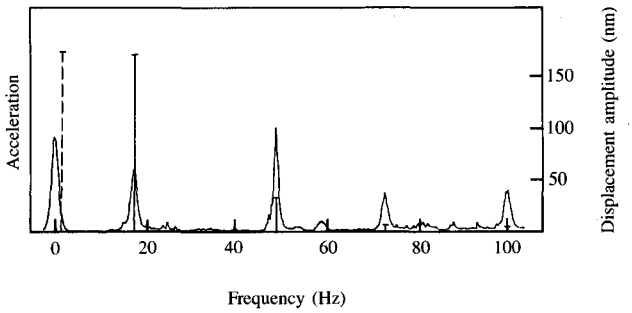

Figure 2

Vibration spectrum of a typical floor in our laboratory. The curve depicts accelerometer output, the solid bars depict corresponding displacement amplitudes, and the dashed bar depicts the effects of walking in the laboratory. The scale at the right pertains to the bars.

• *Damping systems*

The influence on the tip-to-sample distance of the external perturbations described above can be reduced by damping mechanisms and/or sufficient stiffness of the basic STM structure sketched in Figure 1. The stiffer the structure, the less the damping which is needed. This qualitative requirement will now be cast into a quantitative formulation.

The discussion is restricted to simple, passive damping systems. Such systems generally consist of one or more elastic damping elements (dampers) on which the structure to be protected is mounted (Figure 1). For the present discussion, this structure may be considered to be perfectly stiff, and therefore completely characterized by its six mechanical degrees of freedom. Excitation of any one of them may affect the tip-to-sample distance, as is discussed later. Therefore, in principle, the damping effect with regard to each of them has to be considered. Most often, however, only one or two modes contribute significantly, given the design of an STM and the direction of its external perturbations. Since building floors mostly vibrate vertically, we restrict the following discussion to purely vertical translational shaking. It can be extended to more complicated situations by appropriate superposition of rotational and translational modes.

The combined STM/damper structure forms an elastic resonator. Because of the assumed restriction to translational motion here, the structure can be characterized by a single parameter, viz., its mass m_{STM}. The system hence has a single resonance of frequency ν_d. The damper elements are characterized by their elastic constant C_d^* (spring constant) and quality factor Q_d, which is a measure of the amplitude enhancement at resonant excitation and the width of the resonance curve. (Instead of the quality factor, the so-called loss ratio is frequently used in the technical literature.) Losses in a damping system usually have their origins in viscoelastic internal friction (e.g., caoutchouc dampers) and/or external attenuators (e.g., eddy-current damping).

The effectiveness of a damping system can be expressed by its transmittivity $\tilde{t}_d$, defined as the ratio of amplitudes of the supported STM structure $|\hat{z}|$ and excitation $\hat{z}_e$ of the base. Harmonic oscillator theory yields

$$\tilde{t}_d(\Omega_d) = [(\Omega_d^2 - 1)^2 + \Omega_d^2/Q_d^2]^{-1/2}, \quad (2)$$

where Ω_d is normalized to the undamped resonance frequency, viz.,

$$\Omega_d \equiv \nu/\nu_d, \quad (3)$$

and

$$\nu_d = \frac{1}{2\pi}\sqrt{C_d^*/m_{STM}}. \quad (4)$$

Equation (2) is plotted in **Figure 3** for two sets of parameters: Curve $\tilde{t}_{d1}$ results from $\nu_d = 3$ Hz, $Q_d = 3$, which is typical for damping systems with metallic springs and eddy-current attenuation; the respective values for curve $\tilde{t}_{d2}$ are $\nu_d = 5$ Hz, $Q_d = 15$, typical for damping systems with commercial antivibration pads made from caoutchouc.

Three frequency regimes can be recognized in Figure 3: At low frequencies ($\nu < \nu_d$), there is no damping. Near resonance, the damping system enhances perturbations instead of reducing them (unless the system is overdamped). Only above a critical frequency

$$\Omega_{d,cr} = \sqrt{2(1 - 1/2Q_d^2)}$$

$$\simeq \sqrt{2}, \text{ since in general } Q_d^2 >> 1, \quad (5a)$$

does the damping system begin to fulfill its task, i.e., provide a reduction of perturbation amplitude. An amplitude reduction of 10 dB is achieved for

$$\Omega_{d,10} \simeq 2, \quad (5b)$$

beyond which $\tilde{t}_d$ falls off approximately as Ω_d^{-2}.

To isolate the STM efficiently from building vibrations, the resonance frequency ν_d should be as small as possible; $\nu_d < 1$ Hz would be desirable in view of the spectrum of

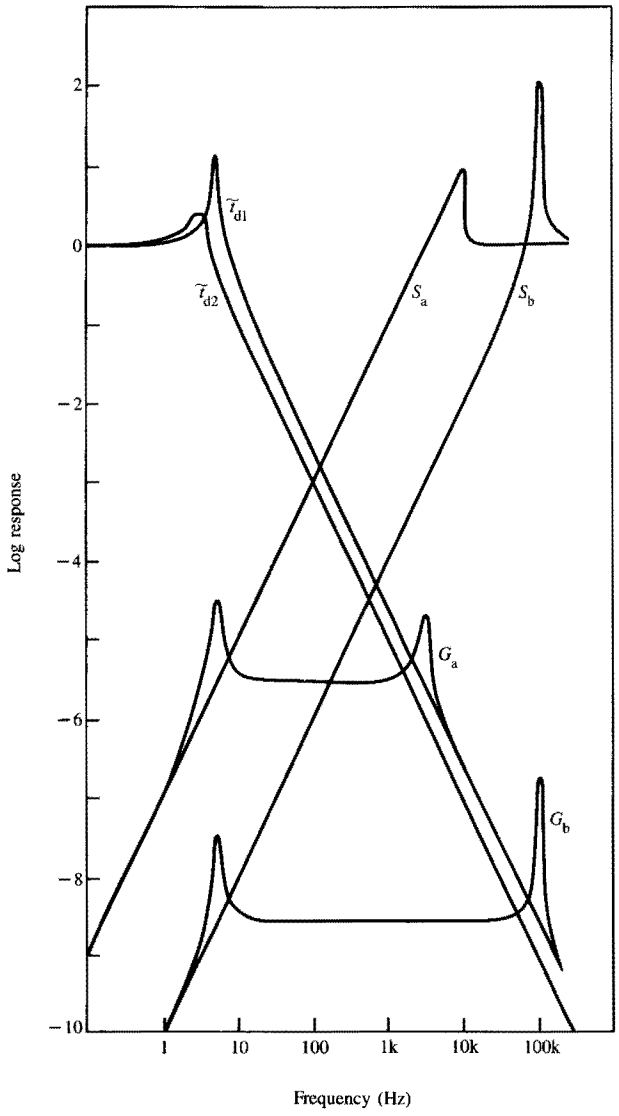

Figure 3

Frequency characteristics of damping ($\tilde{\tau}_{d1}$, $\tilde{\tau}_{d2}$, stiffness (S_a, S_b), and combination of $\tilde{\tau}_{d1}$ with S_a, S_b, (G_a, G_b).

Figure 2. That is difficult to implement, however, because it implies a large static elongation $\Delta z_d(\nu = 0)$ of the elastic element:

$$\Delta z_d(0) = g \cdot m_{STM}/C_d^*, \tag{6}$$

where $g = 9.81\ \text{ms}^{-2}$ is the earth acceleration constant. Comparison with Equation (4) yields

$$(2\pi\nu_d)^2 \cdot \Delta z_d(0) = g. \tag{7}$$

Thus, resonances of 1 and 0.3 Hz would, respectively, require 0.25- and 2.5-m elongations. Such large elongations, though feasible, involve inconveniences of design and operation. Most damping systems, for STMs as well as for other sensitive machinery such as interferometers, therefore operate at $\nu_d = 2$ to 5 Hz.

The quality factor Q_d should not be too large to ensure that accidental excitations at ν_d attenuate within a reasonably short time. On the other hand, it should not be too small to achieve efficient damping for frequencies $\nu > \nu_{d,cr}$. Q_d can be altered with external attenuators such as eddy-current dampers; otherwise, it is necessary to rely on the internal friction of the damping elements. For typical viscoelastic caoutchouc-type elements, $Q_d = 10 - 20$ [2].

It can be seen from Figure 3 that the response to walking remains unattenuated in both cases. The 17-Hz resonance is reduced by 97% in the first case ($\tilde{\tau}_{d1}$) and 90% in the second ($\tilde{\tau}_{d2}$). Thus, amplitudes of about 6 and 20 nm, respectively, appear at the base of an STM when it is excited with the noise spectrum of Figure 2. The 50- and 100-Hz peaks as well as higher-frequency perturbation can be efficiently isolated from the STM by either of the above damping systems. This result is supported by the general experimental observation that noise in the tunneling current is dominated by low-frequency fluctuations.

• *Stiffness and structural resonance*

Large-amplitude low-frequency perturbations which are relatively unaffected by conventional damping systems can jeopardize STM operation unless the STM structure possesses sufficient internal stiffness. Hence, knowledge of the elastic response of the somewhat complex STM mechanical setup can be extremely useful.

The STM structure, being an elastic system, can be characterized by its modes of mechanical excitation and their resonances. As mentioned previously, only those modes which involve motion of the tip relative to the sample influence the tunneling current. The lowest-frequency mode associated with tip motion normal to the sample surface is particularly important.

Qualitative and even semi-quantitative information regarding that mode can usually be obtained by a straightforward analysis. For example, the structure of Figure 1(a) may be expected to show vibrations of the cover plate relative to the base caused by elongation of the connecting rods and/or bending of the plate itself. Calculation of the respective resonance frequencies is unproblematic for simple shapes using expressions which can be found in any textbook on technical mechanics [3].

The critical resonances can also be determined experimentally by subjecting the STM to vibrations from a mechanical shaker and analyzing the frequency spectrum of the tunnel current (cf. Figure 6 of [4]). The lowest-order critical resonances are usually found to be in the 1- to 10-kHz range. The dominance of this frequency regime is a consequence of present-day STM dimensions, typically a few

centimeters, and the materials from which they are fabricated—mostly steel and piezoelectric ceramics.

What are the implications of these resonances for the very low-frequency excitations with which we were previously concerned? To answer this question, we consider the equivalent model depicted in **Figure 1(b)**. It is characterized by a single spring constant C_1^*, load m_1, and quality factor Q_1. The bottom plate of the STM oscillates with amplitude $|\hat{z}(\nu)| = \tilde{t}_d(\nu) \cdot \hat{z}_e(\nu)$ determined previously. The response $z_1(\nu)$ of the top plate can be calculated in a manner following the discussion on the damping system. This time, however, we are interested in the amplitude difference $\Delta\hat{z}_1 \equiv \hat{z}_1 - \hat{z}$ of the top and bottom plates. Normalization to the excitation $\hat{z}$ yields the stiffness transfer function

$$S \equiv |\Delta\hat{z}_1|/\hat{z}. \tag{8}$$

If the damping force determining Q_1 is proportional to the velocity dz_1/dt, the complex amplitude ratio is

$$\hat{z}_1/\hat{z} = [(1 - \Omega_1^2) + i\Omega_1/Q_1]^{-1}. \tag{9a}$$

More commonly, however, the damping force is proportional to $d\Delta z/dt$, resulting in

$$\hat{z}_1/\hat{z} = (1 + i\Omega_1/Q_1)/[(1 - \Omega_1^2) + i\Omega_1/Q_1]. \tag{9b}$$

Here $\Omega_1 \equiv \nu/\nu_1$ denotes the frequency normalized to resonance $\nu_1 = \sqrt{C_1^*/m_1}$. The stiffness factor S calculated from (9b) is also plotted in Figure 3. The S_a curve, with $\nu_1 =$ 3 kHz, $Q_1 = 30$, is typical for present-day STMs consisting of several-cm-size structures made of piezoelectric ceramics and steel. The S_b curve, with $\nu_1 = 100$ kHz, $Q_1 = 100$, represents about the best stiffness one can expect for STMs with piezoelectric ceramic scanners (cf. Section 3).

At low frequencies, expression (8) reduces to

$$S(\Omega_1 \to 0) \simeq \begin{cases} \Omega_1/Q_1 = \nu/\nu_1 Q_1 = \mathrm{Im}(\hat{z}_1/\hat{z}), & \text{(10a)} \\ \Omega_1^2 = (\nu/\nu_1)^2 = 1 - \mathrm{Re}(\hat{z}_1/\hat{z}) & \text{(10b)} \end{cases}$$

for the two cases considered (Re and Im denote real and imaginary parts, respectively). This is the low-frequency tail of the stiffness curves in Figure 3 [according to (10b)]. One recognizes that with a structure associated with S_a (hereafter designated as A), about $3 \cdot 10^{-5}$ of the 17-Hz excitation translates into a tip-sample distance disturbance, and 10^{-7} of the "walking" perturbation at 1 Hz. The respective data for structure B (associated with S_b) are $2 \cdot 10^{-8}$ and 10^{-10}, which is much more favorable.

The global instrument response to vibrations is obtained by multiplication of the damping and stiffness transfer functions. The resulting curves G_a and G_b in Figure 3 clearly indicate the frequency regimes which are problematic with regard to external perturbations.

The transformation of external vibrations into tunneling-distance variations is illustrated in **Figure 4**. The upper curve is a model noise spectrum with the features of the spectrum shown in Figure 2 plus an arbitrary $1/f$ background. The

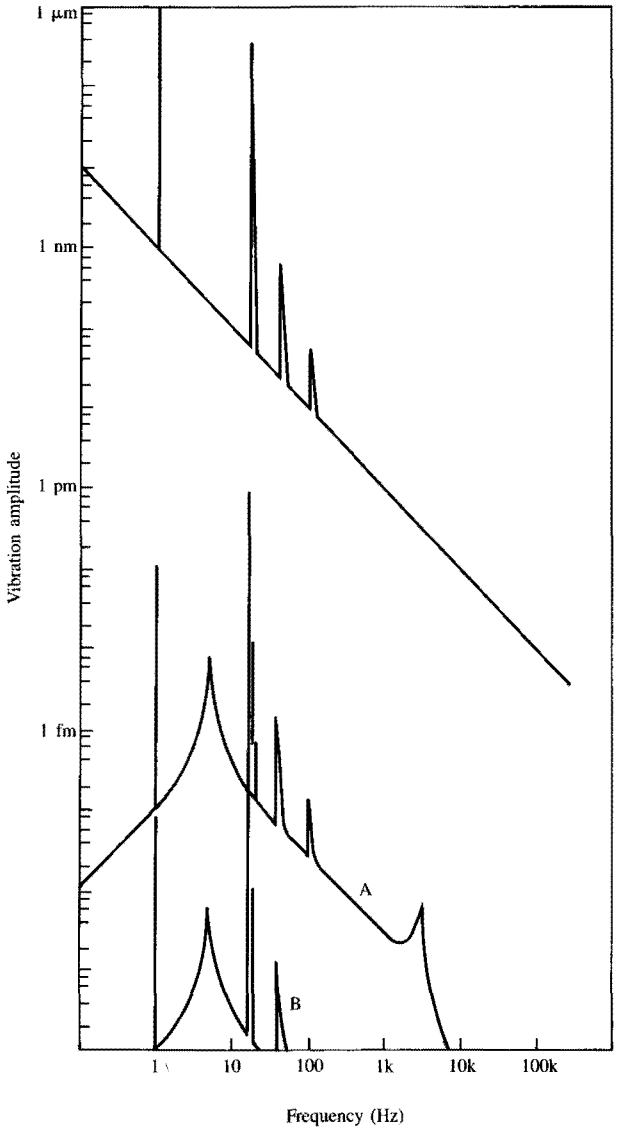

Figure 4

Model noise spectrum (upper curve) and its transformation into tip-to-sample vibration amplitudes for STMs A and B.

lower curves show the resulting uncontrolled motion of tip vs. sample for STMs A and B and $\nu_d = 5$ Hz, $Q_d = 15$ ($\tilde{t}_{d2}$), and for damping force proportional to velocity difference. One recognizes that the 17-Hz vibration amplitude for A just meets the tolerance of 1 pm. This means that any small extra excitation in this frequency range is sufficient to create noticeable perturbations in the tunneling current. This finding agrees with the experimental observation that highest-quality results can be obtained at quiet times of the day (night) only. Walking noise remains well below the limit unless excessive amplitudes are created, for instance, by jumping on the floor. Setup B, on the other hand, provides

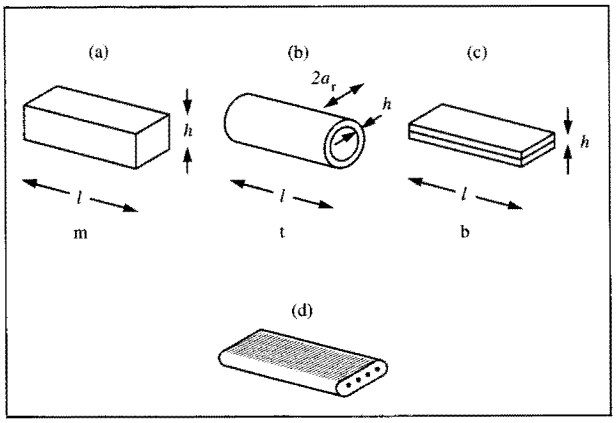

Figure 5

Common piezoelectric ceramic construction elements: (a) Massive cantilever beam, m. (b) Tube, t. (c) and (d) bimorphs, b.

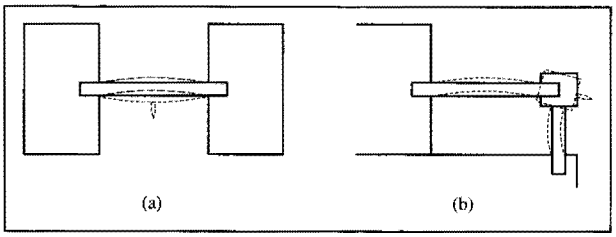

Figure 6

Mounting of piezoelectric ceramic elements and lowest-order vibrational modes. (a) Linear arrangement with both ends clamped. (b) Tripod arrangement.

such a large amount of stiffness that in fact one could expect to operate it directly on the floor without any damping installations!

Figures 3 and 4, as well as the results of the preceding discussion, suggest raising the lowest critical resonance to at least 10 kHz in order to safely meet tolerance requirement 1. Alternatively, achieving an increase in Q_1 would be difficult and actually undesirable since accidental perturbations at ν_1 could have catastrophic consequences in this case.

The use of small STM components and rugged design appears to be the most practical strategy to displace resonances to high frequencies. In the next section, an inherent limitation to the reduction of component dimensions is discussed.

3. Displacement capability and stiffness

Tip, sample, sample holder, etc. in an STM can be made almost arbitrarily small. The piezoelectric ceramic elements usually employed for the six (five) translations, however, require a certain minimum length to provide the range of displacement desired. This results in a trade-off between the requirements of maximum resonance frequency and minimum feasible translation. In the discussion of this problem, we restrict ourselves to the scanner head.

Three types of piezoelectric elements will be compared: massive cantilever beam (m), tube (t), and bimorph or bender element (b) [5]. (Tubes operating in the "dog-tail mode" [6] are very similar in their performance to the thin bimorphs considered here.) The three types, shown in **Figures 5(a)–(d)**, are commercially available. Beams and tubes generally operate in the longitudinal mode. Bimorphs bend sideways, which results in a large increase of amplitude for a given voltage. The increase is obtained at the expense of driving force and stiffness, however, which reduces the permissible load. The bimorph shown in Figure 5(c) is a laminate of two sheets of piezoelectric ceramic material with an intervening metal sheet [7a]. The bimorph in Figure 5(d) is a monolithic sintered structure with thin wires as center electrode [7b]. The displacement Δx vs. voltage U relation [5] for massive beam and tube is

$$\Delta x_{m,t} = d_{31} U l/h. \tag{11a}$$

The respective relation for a bimorph clamped at both ends is

$$\Delta x_b = d_{31} U \cdot \frac{3}{8}(l/h)^2. \tag{11b}$$

Here, d_{31} is the relevant piezoelectric coefficient, and l and h are the lengths and thicknesses, respectively, of the piezoelectric elements. In most STM scanner designs such as the original tripod [1], the "window frame" of [4], or the bender square of [8], the active piezoelectric ceramic element is firmly supported at its ends, as indicated in **Figures 6(a)** and **(b)**. The lowest-order bending mode therefore has nodes at the ends and a maximum at the center. Excitation of this mode affects the tip position by rotation of the tripod end in the first example, and directly as tip-sample distance variation in the latter two. The relation between the dimensions of the unloaded piezoelectric element and the lowest-order bending resonance ν_1 (both ends firmly fixed) [3] for massive cantilever beam and bimorph is

$$\nu_{1(m,b)} = Ch/(l^2\sqrt{3}); \tag{12a}$$

for the tube, it is

$$\nu_{1(t)} = Ca_r/(l^2\sqrt{2}). \tag{12b}$$

The constant C depends on the elastic modulus E and the density ρ of the piezoelectric ceramic element; viz.,

$$C = (9\pi/16)\sqrt{E/\rho} \simeq 5200 \text{ m/s}. \tag{12c}$$

Combining Equations (11) and (12) casts the resonance/displacement trade-off into the following mathematical shape:

$$\Delta z_m \cdot \sqrt{\nu_1} = d_{31} U \sqrt{C/h\sqrt{3}}, \tag{13a}$$

$$\Delta z_t \cdot \sqrt{\nu_1} = d_{31} U \sqrt{C a_r/\sqrt{2}}/h, \tag{13b}$$

$$\Delta z_b \cdot \nu_1 = d_{31} U \sqrt{3} C/h. \tag{13c}$$

Equations (13) permit the determination of the maximum possible displacement at a given resonance frequency and voltage. In **Figure 7**, curves BU (bending unloaded) illustrate the derived relation for the following frequently used and commercially available cross sections:

Cantilever beam: 3×3 (mm)^2.
Tubes: 6.25-mm diameter, 0.8-mm wall.
Bimorph [7a]: 0.52×6.25 mm.

The voltage values are the maximum permissible ones which scale approximately with thickness h of the piezoelectric ceramic material. The lengths l of the scanner elements, depending on the resonance only, are indicated. The curves for beams and tubes, differing only in their cross sections, have the same $-1/2$ slope. However, tubes produce about twice the maximum voltage performance in the present example because of their larger bending stiffness and smaller wall thickness. The bimorph displacement, involving the same motion as the bending mode, falls off linearly with ν_1 but starts from a very low-frequency value.

Bimorphs are superior in the BU mode to beams below 30 to 60 kHz and to tubes below 10 kHz. Moreover, they only require up to 150 V for operation. Thus, the complications of high-voltage electronics can be avoided by the use of bender elements. Reference [7] describes a low-voltage STM built with such elements.

One recognizes further that the displacement capability of present-day 1–10-kHz STMs is several μm in principle. Since values of, say, 300 nm are sufficient for most applications, a sizable increase in resonance frequency, hence stiffness, may be achieved with smaller STMs, in particular with tubes and bimorphs as design elements.

For high frequencies, lengths and masses of the piezoelectric elements become very small. For this reason, the influence of loads such as tip and tip holder or other parts of the scanner become increasingly relevant. Curve BL in Figure 7 shows the displacement resonance characteristics for a center-loaded, massless bimorph with the same elasticity as before for comparison. The load is $M = 1$ g in this particular example. The curve is calculated from the easily derived relation

$$\Delta z_b \cdot \nu_1^{4/3} = 1.5 d_{31} U (4Ew/\pi M)^{2/3}, \tag{14}$$

with $E = 7 \cdot 10^{10}$ N/m^2 and $w = 0.06$ m. The reduction becomes sizable for $\nu > 100$ kHz, where the load is large compared to the mass of the bimorph.

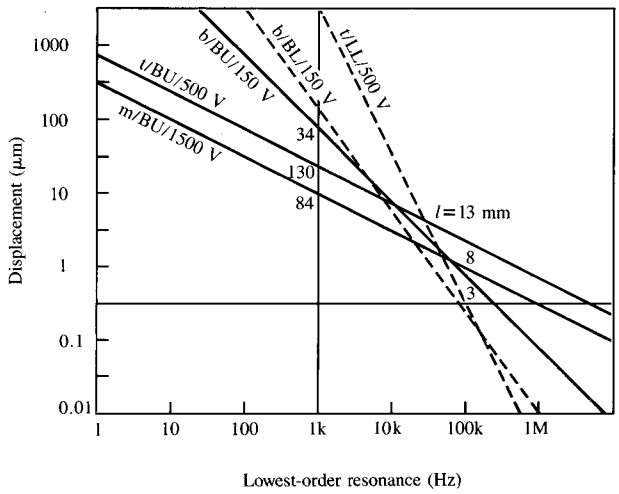

Figure 7

Performance characteristics reflecting the trade-off between displacement capability and stiffness. BU = bending unloaded; BL = bending with load; LL = elongation with load.

Another low-frequency mode to be considered in piezoelectric ceramic scanner elements is longitudinal elongation. In this case, the relation between Δz and ν_1 is

$$\Delta z \cdot \nu_1 = 4 d_{31} U/h\sqrt{E/\rho}. \tag{15}$$

The 1-g load curves for massive beam and tube have also been introduced in Figure 7 (curve LL). The respective bimorph curve would be too large to fit into the graph and therefore is irrelevant.

The LL mode restricts the scanner performance in a manner which is similar to the center-loaded bender mode. One may conclude, therefore, that operation above 100 kHz would be difficult to achieve with piezoelectric ceramic elements unless the tips etc. were shrunk to microscopic dimensions.

4. Drift, hysteresis, and creep

• *Thermal effects*

The relative positions of tip and sample should be close to constant for a given scanner setting during an STM experiment; otherwise, the image appears to drift away and/or become distorted in the direction of drift. This is problematic in particular when a surface is to be scanned slowly in order to arrive at the highest possible resolution.

A major source of drift can be the slow temperature variations of an STM. Assume, for instance, that the mounts of the STM in Figure 1 are fabricated from steel, while the two three-dimensional translator units consist of piezoelectric ceramic material. The mounts may be $l_M = 30$

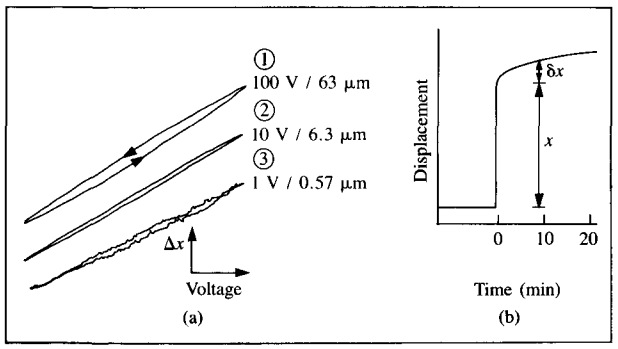

Figure 8

(a) Voltage/displacement characteristic of a 1.5-in. bimorph (R152P). (b) Creep of a piezoelectric tube after step excitation (after [9], reproduced with permission). Material: Vernitron PZT4.

mm in length, for example. The space between the translator units will be small compared to that length.

Under these conditions, any temperature change ΔT would translate into a tip-to-sample distance change of

$$\Delta z_1 = \Delta\alpha \cdot l_M \cdot \Delta T \simeq 300 \text{ nm/K}. \quad (16)$$

Here, thermal expansion coefficients for steel and piezoelectric ceramics of $16 \cdot 10^{-6}$ K^{-1} and $7 \cdot 10^{-6}$ K^{-1} [5], respectively, were used. Satisfaction of tolerance limit 1, i.e., drift $\leq$1 pm, would require the enormous temperature stability of roughly

$$\Delta T \simeq 10^{-5} \text{ K}. \quad (17)$$

Such a high degree of stability is hard to achieve, even for short periods of time. Therefore, it is necessary to make the STM less sensitive to temperature variations or allow for larger tolerances with regard to slow drifts.

An obvious means to deal with the drift problem is to reduce $\Delta\alpha$ along the path from tip to sample. Without temperature stabilization, a nearly perfect temperature compensation would be needed to arrive at drift-free operation. Assume, for instance, a temperature drift of $\partial T/\partial t = 0.1$ K/h and a 3-min duration for one experimental run. Under these conditions, requirement 1 translates into

$$\Delta\alpha \leq 10^{-8} \text{ K}^{-1}. \quad (18)$$

Since a typical STM is much more complex than that depicted in Figure 1, satisfaction of (18) requires careful design.

Symmetric arrangements such as those described in [4] and [7] are favorable for this purpose, in particular with regard to the lateral directions. Compensation with dummy scanner elements as in [4] (z drive) is another favorable approach. It is also necessary, however, to compensate for the tip and sample as well as for the different parts of the rough translation mechanism and the mounting base.

Another source of thermal drift is the temperature dependence of the piezoelectric constant. A typical value is [5a]

$$\partial d_{31}/d_{31}\partial T \simeq 10^{-3} \text{ K}^{-1}. \quad (19)$$

There are exceptions such as the Philips PXE4 material with its almost vanishing temperature coefficient, but this material is not generally available. The drift produced by this effect is proportional to the applied offset voltage and displacement. Considering a value of $\Delta x = 100$ nm as typical, one finds that

$$\partial x/\partial T = 0.1 \text{ nm/K}. \quad (20)$$

Although this value is small with regard to the unbalanced thermal expansion effect, Equation (16), it could become a limiting factor in an STM with well-compensated thermal expansion. The effect can be minimized by choosing temperature-insensitive piezoelectric materials or by correcting the voltage applied to the piezoelectric element in accordance with its predetermined temperature variation. A temperature sensor should be incorporated into the STM for this purpose.

• *Hysteresis and creep of piezoelectric ceramics*

Piezoelectric hysteresis is a disturbing factor in STM operation. The width of the hysteresis loop increases with increasing electrical field. This is illustrated in **Figure 8(a)**, which shows three voltage/displacement loops of a bender element [7] which were obtained for voltage swings of 100, 10, and 1 V, respectively. For the latter two cases, with maximum fields of 50 and 5 V/mm, respectively, hysteresis was almost negligible compared to the first run (500 V/mm). Therefore, it is desirable to employ scanner elements which provide the largest possible ratio dx/dE, where x is the displacement and E the value of the electric field. This small electric-field requirement for a given displacement can be best satisfied with long piezoelectric elements. Thus, as in Section 3, a trade-off has to be made between the requirements for maximum stiffness and minimum electric field.

Another disturbing factor in the operation of piezoelectric ceramics is slow creep after a fast voltage change. **Figure 8(b)**, taken from [9], illustrates the situation. The displacement increases by 20 to 30% within half an hour after the applied step function. As in the case of the hysteresis, the creep increases with increasing amplitude of the electric-field jump. This is a further argument for operating at low electrical fields.

The relation between $E = U/h$ and the lowest-order resonance can be derived from Equations (13). The characteristics for a fixed piezoelectric-element displacement of 1 μm have been plotted in **Figure 9**. The relatively small values associated with curve b indicate that bimorphs again

are the optimum choice—also with regard to hysteresis minimization. As a typical value for the onset of stronger hysteresis, one may assume $E = 100$ V/mm (the horizontal line in Figure 9). The bimorph element reaches this value at 100 kHz. The tube and massive beam elements arrive at this level in the 1- to 10-kHz range.

5. Electronic control system

Our final considerations deal with the optimization of the electronic feedback control needed for tip-to-sample distance regulation. This problem is intimately related to the stiffness considerations discussed in Section 2.

As in any control problem, one first has to analyze the "plant," i.e., the system to be controlled. In the case of the STM, the plant consists essentially of the z piezoelectric element and the tip-sample tunneling contact. Combination of the two forms a nonlinear electrical element. It is therefore convenient to locate the tunneling contact, current/voltage converter, and logarithmic amplifier as indicated in **Figure 10** in order to make the plant linear. The latter two elements as well as the tunneling junction are essentially frequency-independent in the regulation range, which would not exceed 30 to 100 kHz. The frequency response of the z piezoelectric element is characterized by the elastic resonances previously discussed. Limiting ourselves to the lowest-order resonance, we arrive at the Bode plot of **Figure 11** for the plant. Here, a low-frequency gain of 100 and a resonance at $\nu_1 = 3$ kHz have been assumed. These values refer to one of our earlier STMs; they must be determined individually for every STM and sample material.

The controller, i.e., the electrical feedback circuitry, must achieve large gain at $\nu \rightarrow 0$, sufficient attenuation near ν_1, and crossover (gain = 1) at a frequency as high as possible. The first requirement guarantees precise positioning; the second prevents oscillations; and the third ensures fast response. Two open-loop Bode plots satisfying these requirements are also shown in Figure 11 (central solid and dashed curves). Subtraction of the plant plot provides the desired controller response (lower solid and dashed curves).

In the solid curves for open loop and controller, one recognizes a low-frequency part with integrator characteristics and a high-frequency part with the characteristics of a high-order low-pass filter. The cutoff frequency (gain = 1) is chosen to provide a phase reserve of 45°, as is usual in control design. The steep low-pass filter increases the cutoff frequency considerably compared to a pure integrator, indicated by dashed lines in Figure 11.

The cutoff frequency limits the recording speed for the integrator low-pass combination to about 1 kHz, i.e., $\sim\nu_1/3$. In order to achieve higher speeds—a very desirable goal with regard to efficiency, stability, and convenience—the elastic resonances should be pushed to values as high as possible. In the previous discussion, we have seen that ν_1 might be raised to values between 30 and 100 kHz. One could then expect to regulate with a speed of up to 10 to 30 kHz. The record of a full TV frame with 500 × 500 pixels could hence be achieved within 10 to 30 s; when operating in the average mode [10], the speed might be increased to 20 frames per second. This would allow surface observation at scanning speeds comparable to those of an SEM, thus opening fascinating new fields of application.

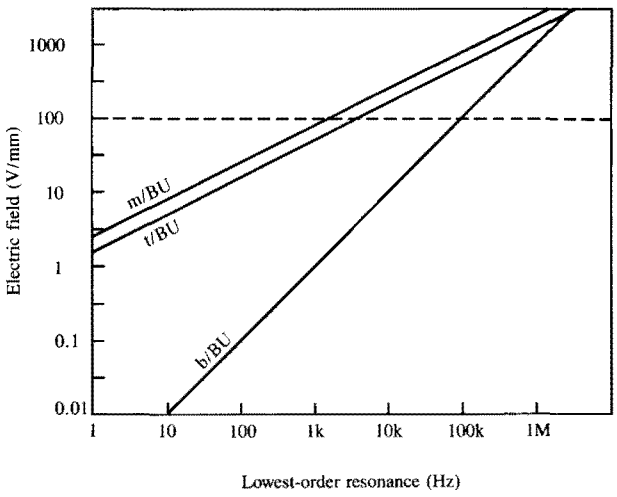

Figure 9

Performance characteristics at a piezoelectric element displacement of 1 μm, reflecting the trade-off between electric field and stiffness.

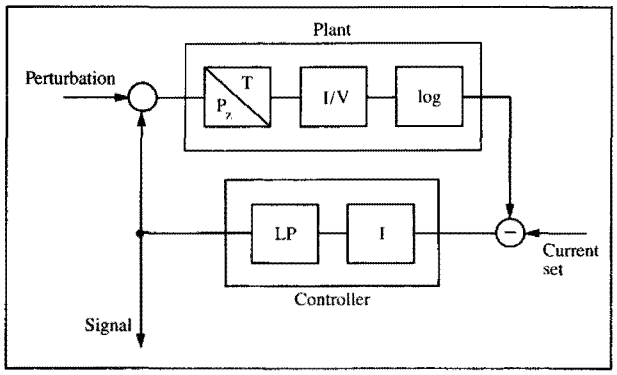

Figure 10

STM closed-loop control system: piezoelectric element (P_z), tunneling junction (T), current/voltage converter (I/V), logarithmic amplifier (log), integrator (I), and low-pass filter (LP).

6. Summary

Tip-to-sample distance tolerances and a set of further essential mechanical requirements have been defined. The

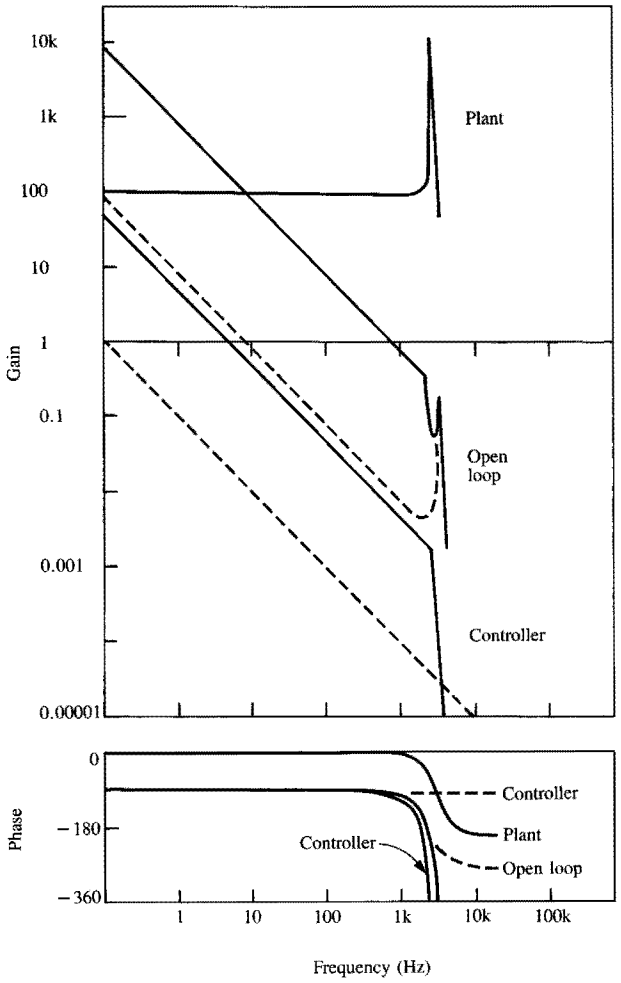

Figure 11

Bode plots of STM plant, controller, and open-loop system. Solid curves: integrator plus low-pass filter; dashed curves: integrator only.

roles of building vibrations, damping, and stiffness have been analyzed. In present-day STMs use is made of a certain amount of damping to reduce building-induced vibrations to a tolerable level. This requirement might be lessened in future designs by decreasing the dimensions of STMs and increasing their stiffness.

Consideration of piezoelectric displacement and elastic resonances has indicated the necessity for trade-offs between the requirements for stiffness and displacement capability. Such trade-offs have been illustrated in design charts for massive cantilever beams, tubes, and bimorphs as piezoelectric translators—indicating that bimorphs provide optimum operating conditions. Tubes operating in the longitudinal mode are the second-best choice. An upper frequency limit for feedback-controlled STM operation might be expected around 100 kHz.

Relatively slow perturbations to STM operation result from temperature drift, piezoelectric hysteresis, and creep. The influence of thermal effects can be minimized by sufficiently reducing the differential thermal expansion between tip and sample. This can be achieved by use of symmetric arrangements and by careful choice of materials. The effects of the temperature dependence of the piezoelectric constant can be compensated for by using the input from a temperature sensor for adjusting the voltage applied to the piezoelectric element and/or employing appropriate piezoelectric materials.

Hysteresis and creep of piezoelectric materials can be minimized by avoiding the use of large electric-field amplitudes. This requirement conflicts with that for maximum stiffness, leading to the need for a trade-off with regard to electric field and elastic resonance. Again, bimorphs provide the best figures of merit.

Consideration of the STM as a "plant" of a feedback system has led to the development of some design criteria for the electronic control system of an STM. Cutoff frequencies of about 1/3 of the lowest-order resonance frequency may be realized by an optimized controller arrangement. Hence, if optimum stiffness can be achieved, a considerable increase in recording speed may become possible.

Acknowledgments

Numerous discussions with my colleagues at the IBM Zurich Research Laboratory, Rüschlikon, and other locations, particularly those with G. Binnig, U. Dürig, C. Gerber, J. Gimzewski, A. Humbert, P. Muralt, and H. Rohrer, were of great value for this work and are gratefully acknowledged.

References

1. Reviews with extensive references: G. Binnig and H. Rohrer, "Scanning Tunneling Microscopy," *Physica* **127b,** 37 (1984); G. Binnig and H. Rohrer, "Scanning Tunneling Microscopy," *Sci. Amer.* **253,** 50 (1985), and G. Binnig and H. Rohrer, "Scanning Tunneling Microscopy," *IBM J. Res. Develop.* **30,** 231–245 (1986, this issue).
2. See, e.g., E. Ioarmides and P. Grootenhuis, "A Finite Element Analysis of the Harmonic Response of Damped Three-Layer Plates," *J. Sound Vibr.* **67,** 203 (1979).
3. See, e.g., A. E. H. Love, *The Mathematical Theory of Elasticity,* Dover Publications, New York, 1926; W. Weizel, *Lehrbuch der Theoretischen Physik,* Vol. I, Springer, Berlin, 1955.
4. H. van Kempen and G. F. A. van de Walle, "Applications of a High-Stability Scanning Tunneling Microscope," *IBM J. Res. Develop.* (to be published in Sept. 1986).
5. See, e.g., (a) *Piezoelectric Ceramics,* J. V. Randeraat and R. E. Setterington, Eds., Mullard Ltd., London, 1974; (b) J. M. Herbert, *Ferroelectric Transducers and Sensors,* Gordon and Breach, New York, 1982; (c) S. Vieira, "Behavior and Calibration of Some Piezoelectric Ceramics Used in the Scanning Tunneling Microscope," *IBM J. Res. Develop.* (to be published in Sept. 1986).
6. G. Binnig and Ch. Gerber, IBM Research Division, Zurich, private communication.
7. (a) Piezo-Electric Products Inc., 212 Durham Ave., Metuchen, NJ 08840; Type R152P; (b) Philips serial flexure elements.

8. P. Muralt, D. W. Pohl, and W. Denk, "Wide-Range, Low-Operating-Voltage, Bimorph STM: Application as Potentiometer," *IBM J. Res. Develop.* (to be published in Sept. 1986).
9. R. W. Basedow and T. D. Cocks, "Piezoelectric Ceramic Displacement Characteristics at Low Frequencies and Their Consequences in Fabry-Perot Interferometry," *J. Phys. E* **13,** 840 (1980).
10. S. A. Elrod, A. Bryant, A. L. de Lozanne, S. Park, D. Smith, and C. F. Quate, "Tunneling Microscopy from 300 to 4.2 K," *IBM J. Res. Develop.* **30,** 261–269 (1986, this issue).

Received September 4, 1985; accepted for publication December 18, 1985

Dieter W. Pohl *IBM Corporation, Zurich Research Laboratory, Säumerstrasse 4, 8803 Rüschlikon, Switzerland.* Dr. Pohl joined IBM in 1968 after receiving his Ph.D. with first-class honors from the Technical University of Munich, Federal Republic of Germany. In 1962, he operated one of the first lasers in Europe during the investigations for his diploma thesis. At IBM, he worked on problems of nonlinear optics and light scattering for several years. In 1982, he joined the IBM Zurich effort on STM and related techniques. He now heads a project oriented toward the study of materials of technological interest. He is the inventor of the near-field optical microscope, which exploits micromechanical principles developed for STM to obtain optical images with near-electron-microscopical resolution. Dr. Pohl is a member of the European, Swiss, and German physical societies.